RSC Advances

ROYAL SOCIETY OF CHEMISTRY

www.rsc.org/advances

Oxidative Coupling of 2-Naphthol by Zeolite-Y Supported Homo and Heterometallic Trinuclear Acetate Clusters

Sameeran Kr. Das, Sanjeev P. Mahanta and Kusum K. Bania*

Department of Chemical Sciences, Tezpur University, Assam, India, 784028

Abstract: Two trinuclear acetate cluster of iron and cobalt of general formula $[Fe_3O(O_2CCH_3)_6(H_2O)_3]NO_3.2H_2O$ and $Fe_2Co(O)[(OOCHC_6H_4NO_2)_6]NO_3.2H_2O$ are synthesized and characterized. The synthesized trinuclear clusters are supported on zeolite-Y via ion exchanged method. FTIR study reveals that the two complexes are tethered via formation of Si-O-H---O-H hydrogen bond linkage with zeolite-Y matrix. Homogeneous and heterogeneous trinuclear catalysts are found to be efficient catalyst for oxidative coupling of 2-naphthol. Compared to homometallic oxo-clusters, bimetallic complexes are found to show better catalytic activity. Besides obtaining BINOL as a major product, these metal clusters also lead to formation of tautomeric form of the BINOL. The crystal structure of the by-product indicates the formation of a tetrahedral chiral centre in the molecule via the attachment of the solvent. Density Functional Theory (DFT) calculation has been performed to elucidate the structural and electronic properties of both homogeneous and heterogeneous complexes.

Key words: Zeolite-Y, Trinuclear Acetate Cluster, 2-Naphthol, C-C coupling, DFT calculation

1. Introduction: Contemporary interest in the catalytic oxidation of alcohols has fascinated the researchers to develop catalyst which could help in the production of fine chemicals.[1-3] Out of the various catalytic oxidation processes, oxidation of 2-naphthol to BINOL is among the principal target reactions as both (*S*)-BINOL and (*R*)-BINOL are used as chiral auxiliaries in asymmetric synthesis.[4-6] Selective oxidation of 2-naphthol to either (*S*) or (*R*)-BINOL has been achieved using various transition metal catalysts.[7-9] Katsuki and co-worker have reported for asymmetric synthesis of chiral BINOL using chiral iron-Schiff base complexes.[10,11] From our group we also account for role of cation-π interaction in enantioselective conversion of 2-naphthol to *R*-BINOL by zeolite-Y encapsulated Fe-Schiff base complexes.[12] Besides the transition metal complexes recently, various bimetallic transition metal oxides are found to be active for such C-C bond coupling reaction.[13]

Although, some homogeneous catalyst has been found to be effective for such reaction using molecular oxygen as oxidant but there are only few heterogeneous catalysts reported for the oxidative biaryl coupling reaction. Cu^{2+} and Fe^{3+}exchanged exchanged MCM-41,[14,15] Fe^{3+} and Cu^{2+} exchanged montmorillonite,[16,17] and vanadium-Schiff-base/SiO_2[18] are few examples of such heterogeneous catalysts used in the synthesis of biaryl compounds. However, the reported procedures has certain disadvantages in terms of the turnover number, deactivation of catalyst and used of hazardous solvent such as chlorobenzene and chloroform. Matsushita et al[19] reported for a supported ruthenium hydroxide catalyst (Ru(OH)*x*/Al_2O_3) as an effective heterogeneous green catalyst for the aerobic biaryl coupling of 2-naphthols and substituted phenols in water without any additives.

With the aim of arriving at a cleaner, more efficient catalytic system for the production of BINOL from 2-naphthol, we have designed a new catalyst that entails harnessing the advantages of oxo-centered trimeric Fe(III) and Co(III) acetates[20] and zeolite-Y.[21] Oxo-bridged transition-metal carboxylate clusters with auxiliary N- and O-donor ligands are interesting because of their complex and diverse structural motifs.[22] These type of metal complexes are also well known due to their optical, catalytic and magnetic properties.[23,24] They exhibit very good properties as homogeneous catalysts[25] and also act as building blocks for designing of supramolecules.[26] In recent years they have been widely used as precursors for synthesis of mixed metal oxide naoparticles like $CoFe_2O_4$, $NiFe_2O_4$ and spinel ferrite nanoparticles.[27-31]

Zeolite-Y with high pore dimension of 7.4 Å is known to act as suitable host and also as support for transition metal complexes.[32] Zeolite-Y due to their special shape selectivity property allows a convenient route for encapsulation of transition metal complexes.[33] Various different types of transition and organometallic complexes and also transition metal clusters either encapsulated or supported on zeolite-Y are found to be effective heterogeneous catalyst for various chemical reactions.[34-36] Recently, we have reported for applicability of zeolite-Y as superior host in preventing the stability and catalytic activity of a chiral Cu-Schiff base complex.[37,38] Thus looking at the advantages of trinuclear oxo-centered Fe^{III}/ Co^{III} metal oxalates and zeolite-Y, we immobilized two complexes over zeolite-Y via ion exchanged method and used them as catalysts for catalytic oxidation of 2-naphthol. The supported metal complexes are found to convert naphthol to BINOL with high yield.

2. Experimental and Theoretical Methods

2.1. Experimental Section

2.1.1. Materials. The metal salts used for the synthesis of $[Fe_3O(O_2CCH_3)_6(H_2O)_3]NO_3.2H_2O$ and $Fe_2Co(O)[(OOCHC_6H_4NO_2)_6]NO_3.2H_2O$ are $Fe(NO_3)_3.9H_2O$, $CH_3CO_2Na.3H_2O$, $CoCl_2.6H_2O$, m-nitrobenzoic acid. All these chemicals are procured from E-Merck. The electrolyte tetrabutyl ammonium phosphate (TBAP) used are of analytical grade (AR) obtained from E-Merck. NaY zeolites are obtained from HiTech.India Ltd. Solvents are purified by standard procedure prior to use.

2.1.2. Synthesis of $[Fe_3(O)(OOCCH_3)_6(H_2O)_3]NO_3.2H_2O$ (Complex 1). Complex 1 is prepared by mixing $Fe(NO_3)_3.9H_2O$ (10 mmol, 4.04 g) and $CH_3CO_2Na.3H_2O$ (20 mmol, 2.72 g) in a mortar and a paste of the reagents is prepared, Scheme 1. The resultant paste is then transferred to a two neck round bottomed flask. To the paste 30 ml of CH_3OH is added and stirred under refluxing condition. The refluxing is continued for about 12 hrs. After the completion of the stirring, the reaction mixture is filtered and the filtrate is kept undisturbed for crystallization. Dark brown crystals are obtained after a few days.

2.1.3. Synthesis of $Fe_2Co(O)[(OOCHC_6H_4NO_2)_6].3H_2O$ (Complex 2). To synthesize Complex 2, we first prepared sodium 3-nitrobenzoate by dissolving a solution of NaOH (5 mmol, 0.2 g) and m-nitrobenzoic acid (5 mmol, 0.835 g) in methanol. The reaction mixture is stirred for about two hours and an off-white precipitate of is obtained. The prepared sodium 3-nitro benzoate solution is then added to a solution of $Fe(NO_3)_3.9H_2O$ (5mmol, 2.02 g) and $CoCl_2.6H_2O$ (5mmol, 1.19 g) prepared in about 20 ml of CH_3OH in a two neck round bottomed flask, Scheme 1. After stirring the reaction mixture for 4h, a 30% solution of H_2O_2 (V/V, 7 ml, ~70 mmol) is added. The whole reaction mixture is then refluxed for 5 hours.

The reaction mixture is filtered and the filtrate is kept undisturbed for crystallization. Light brownish crystals are obtained after few days,.

2.1.4. Synthesis of Zeolite-Y Supported Trinuclear Oxo-Centered Metal Complexes, Complex 1-Y and Complex 2-Y. Zeolite-Y supported metal clusters are synthesized by ion-exchange method. In a general procedure a methanolic solution of either Complex 1 or Complex 2 in either case (0.05 mmol) is prepared in a round bottomed flask. To this solution, 0.5 g of zeolite-NaY is added and stirred well for 24 hours under reflux condition, Scheme 1. The brown solid product so obtained is then filtered (until it get free from nitrate) and dried under vacuum for 2 days to obtain the zeolite-Y supported metal complexes.

2.1.5. Catalytic Oxidation of 2-Naphthol. The oxidation of 2-naphthol is carried out following the previous reported procedure.[12] In a typical catalytic process, 5 mmol of 2-naphthol along with 10 ml of methanol, 25 mg of catalyst are added into a 100 ml two-necked flask equipped with a condenser and an air pump. The reaction is started by passing the dry air with a stable flow rate of 80 ml /min controlled by a flow meter into the bottom of reactor at reaction temperature. The progress of the reaction is monitored by thin layer chromatography and after the completion of the reaction; the catalyst is filtered, washed with petroleum ether and dried at 100 °C overnight. The amount of iron content in 25 mg of the catalyst is determined according Vogels method.[39] The turn over number is determined by following the equation; TON = [BINOL(mmol)/ Fe-atoms on catalyst(mmol)].

2.1.6. Characterization. Powder X-ray diffraction (XRD) patterns are recorded on a Shimadzu XD-D1 powder X-ray diffractometer using Cu Kα radiation (λ = 1.542 Å). XRD patterns are recorded in the 2θ range of 5-50° at a scanning rate of 2°/min. The electronic absorption spectra are measured using a Hitachi U-3400 spectrophotometer with a diffuse reflectance apparatus equipped with an integrating sphere of 60 mm inner diameter. Mono-

chromatic light is used in the whole spectral region in order to minimize the effect of fluorescence. For recording the spectra zeolite supported metal complexes, the powdered samples are placed in a black absorbing hole (10 mm, in diameter and 3 mm deep) of a sample holder, and the surface is smoothed. The layer can be regarded as infinitely thick, as required by the Kubelka-Munk theory. The optical spectrums are then recorded in the reflectance mode. A Kubelka-Munk (KM) analysis[40] is performed on the reflectance data. The KM factor, $F(R)$, is given by F(R) = (1-R)2/2R = k/s where R is the diffuse reflectance of the sample as compared to $BaSO_4$, k is the molar absorption coefficient, and s is the scattering coefficient of the sample. The infrared spectra in the range of 450- 4000 cm^{-1} are recorded on a Perkin-Elmer Spectrum 2000 FTIR spectrometer. The spectra of the zeolite-supported complexes are recorded against a zeolite background, which is recorded at 100 °C after 1 h of evacuation at 10^{-2} Torr. The spectra of the free complexes are recorded as KBr pellets. The SEM and elemental chemical analyses are performed by using JEOL JSM-6390 LV at an accelerated voltage of 5-10 kV. TEM analyses are performed by using JEOL, JEM 2100 at an accelerating voltage of 200 kV. The samples are deposited on a brass holder and sputtered with platinum. CHNS/O-analyser, Perkin Elmer is used for elemental detection. Thermo gravimetric analysis are performed on simultaneous TG-DTA thermo analyzer, Mettler Toledo, with a Pt crucible, Pt/Pt-Rh 13% thermocouples and flow rate of the controlling gas (air) of 20 mL/min. The cyclic voltammograms of neat and supported complexes are recorded on a CHI-600A meter from CH Instruments. TBAP (tetra butyl ammonium phosphate) 0.1 M is used as the supporting electrolyte. The zeolite modified glassy carbon working electrode (ZME) is prepared by dispersing 10 mg of metal complexes in 1 ml of DCM. This suspension is ultrasonicated for 15 min. Ten microlitres (µl) of this dispersion is coated on glassy carbon and 5 μL of 5% styrene (as binder from Aldrich) is

added on these coating and dried in air. The Ag/AgCl/KCl (saturated) is used as reference electrode. The cyclic voltammogram of neat complexes are taken in solution mode, using 0.01M solution of the metal complexes with 0.1M solution of TBAP as supporting electrolyte. MAS-NMR measurements are performed on Bruker ultrasheld 500 MHz WB NMR spectrometer at 11.75 T field producing ^{13}C and ^{29}Si Larmor frequencies at 125.77 and 130.31 MHz respectively. The samples are analyzed by placing in a 3.2 mm zirconia rotor by regulating the spinning speed at 10 KHz. The applied pulse width corresponding to an angle of $\pi/2$ for both the nuclei is 2.3 μs, with a recycle delay of 3s. The chemical shift reference for ^{13}C spectrum is set at 77 MHz corresponding to $CDCl_3$ peak, and for ^{29}Si the reference is set at 0 ppm corresponding to the TSP single peak. Solid state EPR spectra in are recorded on a Bruker ER 200D-SRC X-band spectrometer equipped with an Oxford ESR 9 cryostat. X-ray reflections are collected on a Bruker SMART CCD diffractometer using Mo Kα (λ =0.71073 Å) radiation. Data reductions are performed using Bruker SAINT software.[41] Intensities for absorption are corrected using SADABS. Structures are solved and refined using SHELXL-2008[42] with anisotropic displacement parameters for non-H atoms. All C-H atoms are fixed geometrically using the HFIX command in SHELX-TL. A check of the final CIF file using PLATON[43,44] do not show any missed symmetry. Crystallographic cif file (CCDC 1015210) are available at www.ccdc.cam.ac.uk/.

2.1.7. Computational Method. DFT calculations are carried out using the DMol3 program[45] with VWN correlation functional and double numeric (DN) basis set. The zeolite clusters generated by taking 40 tetrahedral units (40T) of faujasite structure around the supercage, saturating them with hydrogen atoms. Initially, the framework Si and O atoms of the clusters are held fixed at their crystallographic positions and all the terminal H atoms are optimized. Following Löwenstein's rule, one silicon atoms of the six-member ring are

replaced with one aluminium atoms. The gas phase optimized complexes are then encapsulated inside the supercage at several orientations. The negative charge generated in the cluster is compensated by the positive charge of the complexes. While optimizing the clusters, terminated hydrogen atoms are held fixed at their initially optimized positions.

3. Results and Discussion

3.1. Elemental Analysis. In order to confirm the exchange of metal complex with NaY we first estimate the amount of metal content and also C, H and N contents in the two heterogeneous systems. EDX, AAS, and CHN techniques are used for such analyses. Results of the elemental analyses are given in Table 1. EDX study of parent NaY zeolite gives Si/Al ratio of 2.76, which corresponds to a unit cell formula Na_{52} $[(AlO_2)_{52}(SiO_2)_{140}]$. This ratio remains same on ion-exchanged with the cationic complexes. The amount of metal contents determined by various techniques as depicted in Table 1 indicates that on ion exchanged there occurs a loss certain amount of metal contents. This is often a usual case in heterogenisation of a homogeneous catalyst. There are several reports observing such kind of metal leaching. C, H and N analysis of the complexes are found to be in agreement with the expected one. This further suggest for the successful exchange of the metal complexes with zeolite-Y.

3.2. Powder X-Ray Diffraction, PXRD analysis. PXRD patterns of neat zeolite-Y, zeolite-Y supported iron and iron-cobalt trinuclear oxo acetate cluster are shown in Figure 1. The XRD pattern of the neat zeolite-Y and those supported with metal clusters are same. However, the XRD peaks are found to get slightly shifted due to formation of the trinuclear metal-oxo clusters. This change in XRD pattern suggest for the surface modification of zeolite-Y due to complexation with metal complexes.

3.3. Fourier Transform Infrared Spectroscopy (FTIR). The FTIR spectra of zeolite-Y, neat complexes and zeolite-Y-supported trinuclear oxo-metal complexes are shown in Figure 2 and Figure 3. IR spectra of Zeolite-Y show strong zeolite bands in the region 450-1200 cm^{-1}, Figure 2a and 3a. The strong band in the region 1000-1100 cm^{-1} can be attributed to the asymmetric stretching vibration of (Si/Al) O_4 units.[46] The broad band at the region 1650 and 3500 cm^{-1} are due to lattice water molecules and surface hydroxylic group, respectively. The IR bands of all zeolite-Y supported complexes are weak due to their low concentration and thus can only absorb in the region 1200 to 1600 cm^{-1} where the zeolite matrix does not absorb. The characteristics peaks shown in FTIR spectrum for the complexes in Figure 2 and Figure 3 are assigned in Table 2. It can be observed from Figure 2b and Figure 3b that both the complexes supported on zeolite-Y possesses the similar characteristics bands present in the neat complexes, Figure 2c and 3c. However, there occurs some shifting in the vibrational bands due the interaction of the metal complexes with the zeolite matrix.

The most significant change that is observed in the FTIR spectrum of the two supported complexes is in the OH stretching region of zeolite-Y. The IR spectrum of the parent zeolite-Y sample activated at 550 °C displays three bands in the OH stretching region, at 3744, 3724, and 3607 cm^{-1}. According to the literature,[36,47] the band at 3744 cm^{-1} corresponds to external silanols, and that at 3607 cm^{-1} corresponds to bridging acidic OH groups. The weak band at 3724 cm^{-1} is attributed to internal silanols. On ion-exchanged with Complex 1 and Complex 2, we observe several new peaks in the region of 3700-4000 cm^{-1}, Figure 4a and 4b. In case of Complex 1-Y, we observe peak at 3792, 3850 and 3924 cm^{-1} in addition to a peak at 3742 cm^{-1}, Figure 4a. This is obvious because the co-ordinated H_2O molecules of Complex 1 may interact with Si-OH groups of zeolite-Y in different ways, Figure 5a. The presences of 3742 cm^{-1} however, indicate that all the Si-OH group are not

involved in H-bond formation. In case of Complex 2-Y, we observe vibrational bands at 3742, 3754, 3807, 3851, 3895 and 3961 cm^{-1}, Figure 4b. The appearance different vibrational band indicates that in Complex 2-Y not only H_2O but also NO_2 group of the aromatic ligand are involved in the formation of H-bond with zeolite-Y, Figure 5b. The model describe in Figure 5 is based on our previously reported work.[48]

3. 4. ^{29}Si and ^{13}C NMR Analysis. The heterogeneous trinuclear oxo-metal complex with are further characterized by ^{29}Si and ^{13}C NMR spectroscopy. ^{29}Si NMR spectrum of zeolite-Y shows broad peak in between -97.3 to -99.3 ppm, Figure 6a. However, on complexation with Complex 1, chemical shift values are shifted to -88.3 ppm (Figure 6b) while on complexation with Complex 2 it shifted to -81.7 ppm, Figure 6c. The up field shift in the ^{29}Si –NMR spectrum of zeolite-Y on modification with Complex 1 and Complex 2 indicates that the chemical environment near Si in zeolite-Y does not remain the same. ^{13}C NMR spectrum of Complex 1-Y (Figure 7a), shows signal at 179.0 ppm due to carbon atom of the carboxylate group of acetate moiety co-ordinating with iron centres. The peak at 21.7 ppm corresponds to methyl group of acetate ligand, Figure 7a. This result shows that acetate groups of Complex 1-Y are in similar chemical environment. ^{13}C NMR spectrum of Complex 2-Y shows peak at 169.0, 148.1, 135.1, 131.1, 126.1 and 125.3 ppm corresponding to the aromatic m-nitro benzoic acetate group co-ordinating with the Fe and Co atom of Complex 2, Figure 7b. Results obtained from the solid state ^{29}Si and ^{13}C NMR analysis confirms the formation of heterogeneous Complex 1-Y and Complex 2-Y.

3.5. UV-Vis/DRS spectroscopy. The UV-vis spectrums of the neat complexes are recorded in solution phase whereas those of the supported complexes are measured in solid phase in reflectance mode. The UV-vis spectrum of a methanolic solution of Fe-oxo-cluster, Complex 1, shows bands at 211, 313 and 491 nm. The sharp intense band at 211 nm is due to

$\pi \rightarrow \pi^*$ transition originated from the carboxylate moiety. The bands at 313 and 491 nm are because of the Fe^{3+} ion and can be assigned to $_4T^1 \rightarrow {}_4T^2$ and $_4T^1 \rightarrow {}_4A^1$ transition, (Figure 8a). In the corresponding, Fe-Co cluster, absorption bands are observed at 217, 310, 468 and 613 nm, (Figure 8b). The high energy band at 217 nm is due to $\pi \rightarrow \pi^*$ transition originated from the aromatic ring of m-nitro benzoic acid. The band at 310 nm is due charge transfer transition (MLCT) from metal d-orbital to the π^* orbital of the ligand. The band at 468 nm is for Fe^{3+} ion ($_4T^1 \rightarrow {}_4T^2$) and the band at 613 nm is because of the ligand field transition originated from Co^{3+} ($_1A^1 \rightarrow {}_1T^1$).

The diffuse reflectance spectrums of the supported metal complexes are depicted in Figure 9. The DRS spectrum of Complex1 (Figure 9a) shows bands at 217 nm and 488 nm due to $\pi \rightarrow \pi^*$ and d-d transition originated from the ligand and the metal ion, respectively. The presence of the similar electronic transitions indicates the presence of metal complex on the zeolite-Y surface. DRS spectrum of Complex 2 shows band at 223, 268, 351, 476 and 630 nm, (Figure 9b). This indicates the formation of metal complex on the surface of zeolite-Y. In both the supported complexes the peaks are found to be slightly red shifted in comparison to the neat complexes due to the effect of the zeolite matrix.

3.6. ESR analysis. The type of trinuclear metal complexes discussed in the present work are characterized by an S = 1/2 ground state with an excited state with S = 3/2 at 25 cm^{-1}.[49] ESR spectrum recorded from a powdered sample of Complex 1-Y at 77 K is shows in Figure 10**.** At room temperature we do not observe any ESR signal for the Complex 1-Y. At low temperature i.e. at liquid nitrogen temperature (77K) broad signals are observed with a prominent feature at g~ 2.0 for S= ½ state. The signal at g ~2.0 consists of an absorption peak at g ~2.12 a derivative feature at g ~2.0 and a valley at 1.89. In addition to this a weak signal observed at g ~4.3 is characteristics of Fe^{III} (S= 5/2) complex. In absence of any inter-

trimer interaction a symmetric derivative is expected at g ~ 2.0 for S= ½. However, because of the anisotropic effect may lead to splitting of symmetric line. Thus the splitting of the isotropic g values indicates the presence of weak internuclear interaction. It has been reported that ESR spectra of trinuclear transition metal complexes similar to those of Complex 1 and Complex 2 because of non-Heisenberg interactions and/or single-ion zero-field splitting result in a anisotropic S = 1/2 ground state give rise to ESR signal in the g ~2.0 region.[49]

3.7. Cyclic Voltammogram. The nature of intrazeolite or extrazeolite complexes that are not apparent from spectroscopic evidences can also be obtained from electrochemical study.[50] The voltammogram of a neat Complex 1 in solution mode at a scan rate of 0.1V is shown in Figure 11a. The quasi-reversible reduction process is due to a Fe^{III}/Fe^{II} couple, $[Fe_3^{III}O(O_2CR)_6(H_2O)_3] \leftrightarrow [Fe_2^{III}Fe^{II}O(O_2CR)_6(H_2O)_3]$. It shows the oxidation peak due to $Fe^{II} \rightarrow Fe^{III}$ at -0.075V and the corresponding reduction peaks at 0.152V. Besides this it also shows a second reduction wave at a more negative potential at -1.149V. This wave involves two or more electrons and may correspond to metal centered reduction or to the loss of the central oxygen atoms. The cyclic voltammogram taken at different scan rate indicates a decrease in peak intensity of reduction potential, Figure 11b. In case of zeolite-Y supported metal the oxidation peak is observed at -0.509V and the two reduction potentials are observed at -0.219V and -0.626V, Figure 12a. The change in the redox potential values can be attributed to the effect of zeolite matrix. The reduction peak potentials of Complex 1-Y are also found to depend on scan rate, Figure 12b.

Cyclic voltammogram of Complex 2 shows number of peaks and are found to be scan rate dependent (Figure 13a and Figure 13b). Peak I at -1.048V is due to oxidation of Fe^{II} to Fe^{III}, peak II at -0.683V corresponds to oxidation of Co^{II} to Co^{III}. III and IV is for reduction

of $Fe^{III} \rightarrow Fe^{III}$ and $Co^{III} \rightarrow Co^{II}$ whereas the other two reduction potential wave (V and VI) appearing close to -1.0 V may correspond to metal centered reduction or to the loss of the central oxygen atoms. The redox potential values corresponding to Complex 2-Y are found to differ due to the effect of zeolite matrix, Figure 14a and Table 3. The electrochemical behaviour of the complexes found to depend on scan rate. The intensity of the reduction peak gets diminished with the decrease of scan rate, Figure 14b.

3.8. SEM and TEM Analysis: While synthesizing metal complexes in zeolites the complexes may form inside the cavities or on the surface. SEM technique gives an insight whether the complexes are present on the surface of zeolite. Some representative SEM pictures are shown in Figure 15. Figure 15 represents a typical morphology of the zeolite surface for all the considered systems and it shows the deposition of complexes or the uncomplexed species on the external surface, Figure 15b and Figure 15c. The TEM (Figure 16) also directly reveals the intact porosity of the support after immobilization of the metal complex. Massive agglomerations of smaller particles are observed on the surface of the zeolite-Y. These agglomerates consist of many small crystallites clustered together (Figure 16) to form larger aggregates that are distributed on the support surface.

3.9. TGA Analysis: The TG patterns of parent neat complexes and zeolite-Y supported metal clusters are displayed in Figure 17. The neat Complex 1 has four weight loss steps at about 32, 114, 196 and 300 °C while the Complex 2 shows three weight loss steps at about 93, 335, 418 °C. On the basis of the weight changes, the first weight-loss step in both neat complexes corresponds to the loss of water molecule as an endothermic phenomenon. The second weight loss at 93-114 °C is due to loss of co-ordinated water molecules. The third weight loss at 196 ^{o}C in Complex 1 may be related to the loss of acetate group and that in 300 °C may be due to loss of Fe_2O_3. There is a sharp weight change at 334 °C case of

Complex 2 which is attributed to loss nitro-benzoic acid and that above 418 °C is due to loss of metal oxides. However, for the corresponding immobilized complexes the weight loss extend up to 560 °C. On the basis of thermal analysis data, we may conclude that zeolite-Y supported metal complexes may be treated thermally without any significant decomposition.

4. Catalytic Activity

4.1. Oxidative Coupling of 2-Naphthol by Neat and Zeolite Supported Metal Complexes

The oxidative coupling of 2-naphthol is a representative reaction mode for direct synthesis of 1,1′-binaphthol (BINOL) whose optically pure derivatives are regarded as versatile chiral auxiliaries and ligands in asymmetric synthesis. However, these substances remain largely unstudied because of their difficulties in synthesis. We found that the Fe and Fe-Co cluster complexes tethered via H-bonding in zeolite-Y creates a catalyst that allows highly selective transformation of 2-naphthol to BINOL under aerobic condition without any additive. Catalytic conversion of 2-naphthol to BINOL is effected both by temperature and solvent system. So in order to observe the effect of temperature and solvents, we screened the reaction at different temperature and solvents. For this we consider Complex 1 as test catalyst and perform the reaction in different solvents like methanol, dichlromethane (DCM), dimethylformamide (DMF) and toluene refluxing at 30 °C. Most of the complexes showed very poor or no catalytic activity in these solvents at 30 °C. However, on increasing the temperature up to 45 °C in methanol, the neat complexes give the racemic mixture with moderate yield. Reaction performed at ice cool condition does not show any conversion. Hence, the catalytic reaction by all other three catalysts is monitored at 45 °C in methanol. Interestingly, besides isolating BINOL we also obtained minor product which we crystallized and found to be differ from BINOL. The structure of isolated minor product is shown in Figure 18. The minor product is a tautomeric form of the BINOL possessing a chiral centre

created by the attachment of the solvent moiety. Complex 2 shows high selectivity and gives better yield as compared to the Complex 1. Under the same conditions the catalytic activity of the encapsulated complexes are tested for oxidative coupling of 2-naphthol. It can be seen from the data given in Table 4 that the supported complexes give high percentage yield and selectivity in comparison with the neat complexes. We also observe the effect of catalyst amount on the catalytic process. Up to 10 mg of the catalyst we do not observe any progress of the reaction in TLC test. However, after addition of 15 mg of the catalyst conversion of naphthol to BINOL is observed and maximum conversion is obtained on using 25 mg of the catalyst. On increasing the amount of catalyst no significant enhancement in the catalytic conversion is seen. Therefore, the reaction is performed with 25 mg of the catalysts. Among all the complexes, Complex 2-Y shows good conversion of 2-naphthol to BINOL. Blank experiments carried out without the catalyst under identical experimental conditions do not produce BINOL indicating the participation of the iron and iron-cobalt trinuclear oxo-complexes in the reaction path. The use of stoichiometric amount of complexes as oxidizing agent under nitrogen atmosphere do not yield the product indicating that oxygen is essential for the reaction. The time required for this catalytic conversion is found to be less in case of the encapsulated complexes in comparison to the corresponding neat complexes. Oxidative coupling of 2-naphthol with the neat complexes resulted in the formation of racemic BINOL along with the minor chiral product. Further, we could isolate only 45% to 48% of the desired product in case of the reaction catalysed by Complex 1 and Complex 2. However, oxidative coupling of 2-naphthol with Complex1-Y and Complex 2-Y under similar conditions results > 80%. The catalytic conversion of naphthol to BINOL by Complex 2-Y has also been monitored through UV-vis study. The UV-vis spectrum of 2-naphthol shows its characteristics peak at 290 and 318 nm. However, as the reaction proceeds, we observe

two new peaks at 266, 277 and 288 nm characteristic of BINOL (Figure 19). This further confirms the catalytic activity of the synthesized bimetallic Fe-Co oxo cluster.

4.2. Recyclability Test. The homogeneous trinuclear-oxo clusters could not be retrieved after the oxidation process. However, we could successfully recover the zeolite-Y supported metal clusters. To study the recyclability of supported catalyst during oxidation of 2-napthol, we carry out a few reaction under similar condition with Complex 1-Y and Complex 2-Y. After the first run of the oxidation reaction, the catalysts are separated by centrifugation. Fresh reactants are added to the supernatant. Analysis of the reaction mixture shows no further increase in the conversion of 2-napthol. UV-vis study of the supernatant also gives indication for the absence of trace amount of the metal complex. After separation, catalyst are washed thoroughly with petroleum ether, dried, and subjected to another cycle with fresh reactants under similar conditions. The conversion and % yield are found to be consistent. The above procedure is repeated for three cycles, and we do not observed any substantial loss in the catalytic activity of supported catalyst. This indicates that trinuclear metal oxo-cluters are tightly bound to the silanol group of zeolite-Y. However, after third cycle i.e. in fourth and fifth cycles we observed substantial decrease in the catalytic activity. UV analysis of the supertant indicates leaching of the metal content. The amount of metal loss (Fe) after third and fifth cycle as determined by Vogel's method[39] is given in Table 5. Further, cyclic voltammetry analysis of the separated catalyst shows almost similar behavior neat complexes suggesting the detachment of the metal complexes from the solid support thereby perturbing the catalytic activity of the catalyst. Thus, due to metal leaching and rupturing of the H-bond interaction between the complexes and zeolite-Y moiety leads to substantial decrease in the catalytic activity of the heterogeneous catalyst.

4.3. Theoretical Study

Density Functional Theory calculation (DFT) has been performed on Complex 1 and Complex1-Y in order to understand the structural and electronic difference between the neat and the encapsulated system. The geometrical parameters such as bond length and bond angles obtained from VWN/DN level calculations for the neat and the encapsulated complexes are found to be in good agreement with the available crystal structure of such complexes.[51]

The bond distances between the oxygen atom of silanol hydroxyl group and hydrogen atom of H_2O group ranges from 1.94 to 2.56 Å. These distances are smaller than the sum of the van der Waals radii (2.6 Å) of T-atoms of zeolite and hydrogen atom of water. These results indicate the existence of Si-O…H-O hydrogen bond which is in accordance with our experimental FTIR result. The occurrence of H-bond indicates the possibility of tethering of the metal complex over zeolite surface leading to the formation of a supramolecular host-guest complex.

The HOMO and LUMO orbitals corresponding to those of the neat and the encapsulated complexes are shown in Figure 20. HOMO and LUMO orbitals in neat Complex 1 are concentrated at the metal centre while the same in case of Complex 1-Y are partly distributed over the metal complex and zeolite framework. It can be seen that HOMO orbital in case of Complex 1-Y lies higher in energy than the neat Complex 1. This further reveals the fact since the metal complexes are involved as catalyst in oxidative coupling of 2-naphthol where the rate determining step is the oxidation of Fe^{III} to Fe^{IV} by molecular oxygen therefore this oxidation process will be more feasible in case of Complex 1-Y then in comparison to Complex 1.

Acknowledgement: The author thanks Prof. R. C. Deka, Dept. of Chemical Sciences, Tezpur University for helping in computational study. Dr. Tridip Sarma,University of Hyderabad for help and suggestion.

Contact Author: kusum@tezu.ernet.in

References

1 Y. Zhu, B. Zhao, Y. Shi, *Org. Lett.*, 2013, **15**, 992-995.

2 G. L. H. Tapley, M. J. Silvero, C. J. B. Alejo, M. G. Béjar, C. D. McTiernan, M. Grenier, J. C. N. Ferreira, J. C. Scaiano, *J. Phys. Chem. C*, 2013, **117**,12279-12288.

3 J. V. Sundar, V. Subramanian, *Org. Lett.*, 2013, **15**, 5920-5923.

4 J. M. Brunel, *Chem. Re*v. 2005, **105**, 857-897.

5 Y. Chen, S. Yekta, A. K. Yudin, *Chem. Re*v. 2003, **103**, 3155-3212.

6 J. Brussee, J. L. G. Groenendijk, J. M. Koppele, A. C. A. Jansen, *Tetrahedron* 1985, **41**, 3313-3319.

7 J. Hassan, M. Se´vignon, C. Gozzi, E. Schulz, M. Lemaire, *Chem. Rev.* 2002**, 102***,* 1359-1469

8 Q. X. Guo, Z. J. Wu, Z. B. Luo, Q. Z. Liu, J. L. Ye, S. W. Luo, L. F. Cun, L. Z. Gong, *J. Am. Chem. Soc.*, 2007, **129**, 13927-13938.

9 S. E. Allen, R. R. Walvoord, R. P. Salinas, M. C. Kozlowski, *Chem. Rev*. 2013, **113**, 6234-6458.

10 H. Egami, K. Matsumoto, T. Oguma, T. Kunisu, T. Katsuki, *J. Am. Chem. Soc***.** 2010, **132**, 13633-13635.

11 H. Egami, T. Katsuki, *J. Am. Chem. Soc***.** 2009, **131**, 6082-6083.

12 K. K. Bania, D. Bharali, B. Viswanathan, R. C. Deka, *Inorg. Chem*. 2012, **51**, 1657-1674

13 M. V. Maphoru, J. Heveling, S. K. Pillai, *ChemPlusChem,* 2014, **79**, 99 -106.

14 M. R. Prasad, G. Kamalakar, S. J. Kulkarni, K. V. Raghavan, *J. Mol. Catal. A* 2002, **180**, 109-123.

15 E. Armengol, A. Corma, H. Garcı´a, J. Primo, *Eur. J. Org. Chem.* 1999, 1915-1920.

16 M. L. Kantam, B. Kavita, F. Figueras, *Catal. Lett.* 1998, **51**, 113-115.

17 P. Mastrorilli, F. Muscio, G. P. Suranna, C. F. Nobile, M. Latronico, *J. Mol. Catal. A* 2001, **165**, 81-87.

18 M. Tada, T. Taniike, L. M. Kantam, Y. Iwasawa, *Chem. Commun.* 2004, 2542.

19 M. Matsushita, K. Kamata, K. Yamaguchi, N. Mizuno, *J. Am. Chem. Soc***.** 2005, **127**, 6632-6640

20 R. C. Mehrotra, R. Bohra, *Metal Carboxylates*, Academic Press, London, 1983.

21 M. Heitbaum, F. Glorius, I. Escher, *Angew. Chem. Int. Ed*. 2006, **45**, 4732-4762.

22 C.D. Chandler, C. Roger, M. J. Hampden-Smith, *Chem. Rev.,* 1993, **93***,* 1205-1220.

23 G. Losada, M. A. Mendiola, M. T. Sevilla, *Inorg. Chimi. Acta* 1997, **255**, 125-131.

24 H. Vrubel, T. Hasegawa, E. de Oliveira, F. S. Nunes, *Inorg. Chem. Commun*. 2006, **9** 208-211.

25 S. Murata, M. Miura, M. Nomura, *J. Chem. Soc., Perkin Trans*. 1989, **2**, 617-621.

26 H.E. Toma, K. Araki, A.D.P. Alexiou, S. Nikolau, S. Dovidauskas, *Coord. Chem. Rev*. 2001, **219-221** 187-234.

27 Y.Yuan, L. Chen, R. Yang, X. Lu, H. Peng, Z. Luo, Mater. Lett. 2012, **71**, 123-126.

28 L. Chen, Y. Yuan, H. Peng, X. Lu, Z. Luo, 2012, **67**, 311-314

29 L. Chen, Y. Shen, J. Bai, *Mater. Lett*. 2009, **63**, 1099-1101.

30 K.P. Naidek, F. Bianconi, T.Costa R. da Rocha, D. Zanchet, J. A. Bonacin, M. A. Novak, M. das G. F. Vaz, H. Winnischofer, *J. Colloid Interf. Sci.* 2011, **358**, 39-46.

31 K. O. Abdulwahab, M. A. Malik, P. O'Brien, G. A. Timco, F. Tuna, R. E. P. Winpenny, R. A. D. Pattrick, V. S. Cokerd , E. Arenholze, *J. Mater. Chem. C*, 2014, **2**, 6781-6789.

32 K. K. Bania, R. C. Deka, *J. Phys. Chem*. C, 2011, **115**, 9601-9607.

33 A. Corma, H. Garcia, *Eur. J. Inorg. Chem.* 2004, 1143-1164.

34 D. J. Xuereb, R. Raja, *Catal. Sci. Technol.* 2011, **1**, 517-534.

35 M. Stratakis, G. Froudakis, *Org. Lett*. 2000, **2,** 1369-1372.

36 K. K. Bania, R. C. Deka, *J. Phys. Chem. C*, 2013, **117**, 11663-11678.

37 K. K. Bania, G. V. Karunakar, K. Goutham, R. C. Deka, *Inorg. Chem.*, 2013, **52***,*8017-8029.

38 K. K. Bania, G. V. Karunakar, B. Sarma, R. C. Deka, *ChemPlusChem* 2014, **79**, 427-438.

39 A. I. Vogel, *Textbook* of *Quantitative Chemical Analysis*; Pearson Education Asia, 2002, 6th Ed^{n}, p 394.

40 H. G. Hecht, In *Modern Aspect of Reflectance Spectroscopy*; Wendlandt, W. W. Ed.; Plenum Press: New York, 1968.

41 SAINT Plus (Bruker AXS Inc.: Madison, WI, 2008.

42 BRUKER AXS (v 6.14); Bruker AXS Inc.: Madison, WI, 2008.

43 PLATON, A Multipurpose Crystallographic Tool; Spek, A. L. Utrecht University: Utrecht, Netherland, 2002.

44 A. L. Spek, *J. Appl. Crystallogr.* 2003, **36**, 7.

45 B. Delly, *J. Chem. Phys*. 1990, **92**, 508-514.

46 A. Zecchina, C. O. Arean, *Chem. Soc. Rev.* 1996, **25**, 187-196.

47 K. Chakarova, K. Hadjiivanov, *J. Phys. Chem. C* 2011, **115**, 4806-4817.

48 K. K. Bania, R. C. Deka, *J. Phys. Chem. C*, 2012, **116**, 14295–14310.

49 A. K. Boudalis, Y. Sanakis, C. P. Raptopoulou, A. Terzis, J.P. Tuchagues, S. P. Perlepes, *Polyhedron* 2005, **24**, 1540–1548.

50 V. Ganesan, R. Ramaraj, *Langmuir* 1998, **14**, 2497-2501.

51 K. I. Turte, S. G. Shova, V. M.; Meriacre, M. Gdaniec, A. Yu. J. Lipkowski, J Bartolome, F. Wagner, G. Filoti, *J. Struct. Chem.,* 2002, **43**,108-117.

Table 1. Elemental analysis of NaY, Complex 1-Y and Complex 2-Y obtained from EDX, AAS and CHN analysis. The values are given in weight (%)

	EDX- Analysis						AAS			CHN-Analysis		
Sample	Si	Al	Na	M	C	N	Al	Na	M	C	N	H
NaY	21.4	8.5	7.5	-	-	-	8.59	7.58	-	-	-	
Complex 1-Y	21.4	8.2	5.6	(Fe^{3+}) 2.5	22.1		8.2	5.5	(Fe^{3+}) 2.7	24.1	-	5.0
Complex 2-Y	21.4	8.6	5.4	(Fe^{3+}) 8.4 (Co^{3+}) 4.4	40.4	6.6	8.6	5.3	(Fe^{3+}) 8.7 (Co^{3+}) 4.66	40.5	6.7	2.9

Table 2. FTIR analysis of Zeolite-Y, Complex 1, Complex 2, Complex 1-Y and Complex 2-Y

Compound	**Wave number (in cm^{-1})**	**Band Assignment**
Zeolite-Y	1647, 3461	ν(O-H) lattice water, surface hydroxyl
	1000	ν_{as}(Si-O/Al-O)
	553, 453	ν_s(Si-O/Al-O)
Complex 1	3443	ν_s(O-H)
	2993,2850	ν_s(C-H)
	1747,1638	ν_a(C=O)
	1554	$\nu_a(COO^-)$
	1408	$\nu_s(COO^-)$
	1037	ν_s(CO)+δ(O-C=O)
	663,608	Crystal water
	553	ν(MO)+ν(CC)
Complex 2	1619,1480	ν_a(C=C)aromatic
	1531	$\nu_a(COO^-)$
	1408	$\nu_s(COO^-)$
	1336	ν_s(NO)
	1081-1162	ν_s(CO)+δ(O-C=O)
	629,719,784,923	aromatic ring deformation
	542	ν(MO)+ν(CC)
	475	Ring.def+δ(O-C=O)
Comple 1-Y	3467	ν_s(O-H)
	2928	ν_s(C-H)
	1656	ν_a(C=O)
	1545	$\nu_a(COO^-)$
	1419	$\nu_s(COO^-)$
	1302	$-CH_3$ bending
Complex 2-Y	3431	ν_s(O-H)
	1654	ν_a(C=O)
	1553	$\nu_a(COO^-)$
	1480	ν_a(C=C)aromatic
	1404	$\nu_s(COO^-)$
	1352	ν_s(NO)
	665	aromatic ring deformation

Table 3. Oxidation and reduction potential values obtained from cyclic voltammetry study for Complex 1, Complex 2, Complex 1-Y and Complex 2-Y.

Complexes	E^{1}_{oxd}	E^{2}_{oxd}	E^{1}_{red}	E^{2}_{red}	E^{3}_{red}	E^{4}_{red}	E^{av}_{oxd}	E^{av}_{red}
Complex 1	-0.075	-	0.152	-1.149			-0.075	-0.498
Complex 2	-0.683	-1.048	-0.076	-0.385	-0.911	-1.261	-0.865	-0.658
Complex 1-Y	-0.509		-0.219	-0.626	-	-	-0.509	-0.422
Complex 2-Y	-0.203	-	-0.396	-0.849	-	-	-0.203	-0.622

Table 4. Oxidative coupling of 2-naphthol in methanol at 45 °C

Catalysts	time	(%) yield[a]	Fe-atom in catalyst (mmol) [b]	(%) yield in mmol	TON
Zeolite-Y	72h	Nil	-	Nil	-
Complex 1	72 h	45	0.0062	2.25	363
Complex 2	56h	48	0.0020	2.4	1200
Complex 1-Y	24 h	70	0.0058	3.5	603
Complex 2-Y	18 h	86	0.0018	4.3	2388

The reactions were carried out in methanol with catalyst (25mg) on a 5 mmol scale under aerobic conditions. [a] Determined by chromatographic separation. [b] Amount of Fe-atom in mmol present per 25 mg of catalyst.

Table 5. Amount of Fe leached from zeolite-Y complexes after third cycle.

Run	4	5	6	7
Fe loss [a] (%) in Complex 1-Y	0.68	0.013	0.013	0.014
Fe loss [a] (%) in Complex 2-Y	0.62	0.012	0.010	0.013

[a] *Fe in solution/total amount of zeolite-Y supported complexes.*

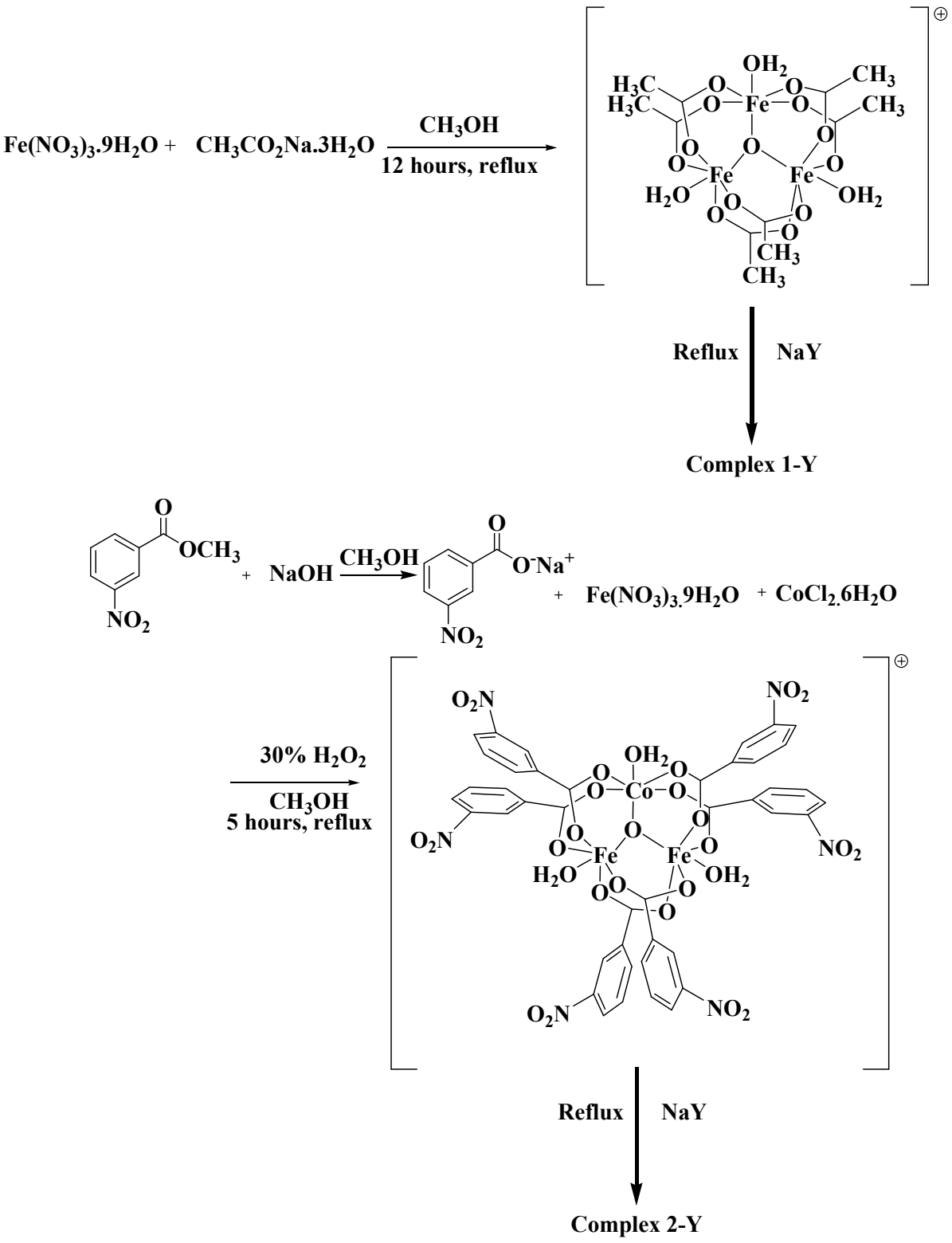

Scheme 1. Synthesis of Complex 1, Complex 2, Complex 1-Y and Complex 2-Y.

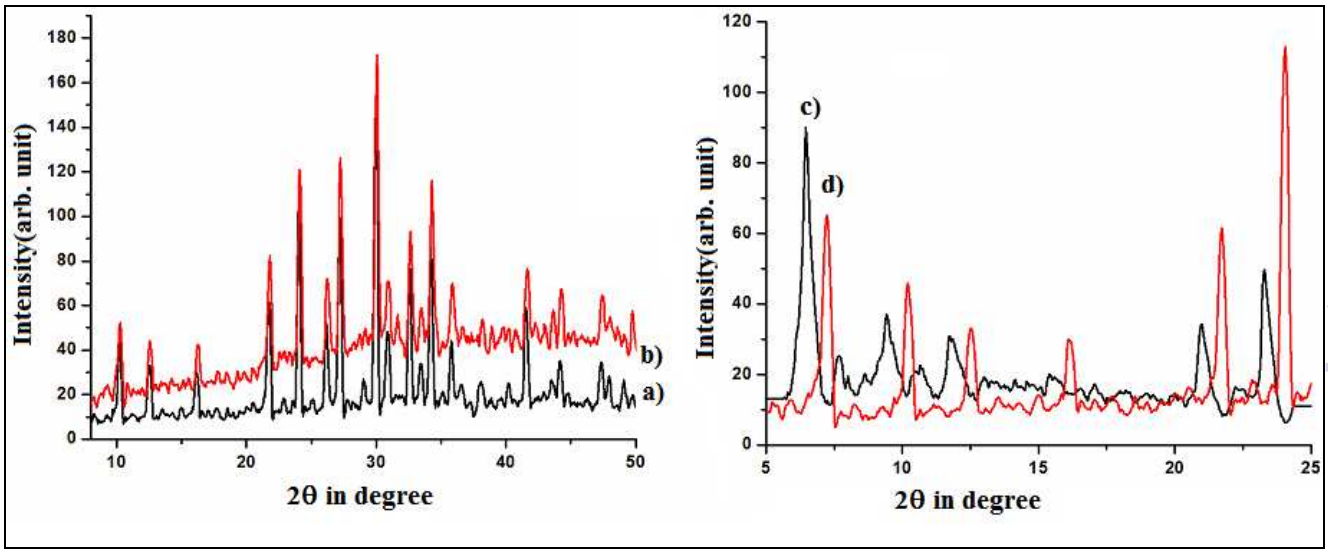

Figure 1. PXRD pattern of Zeolite-Y(black) and zeolite-Y supported metal complex (red). c) and d) are expanded form of a) and b), respectively.

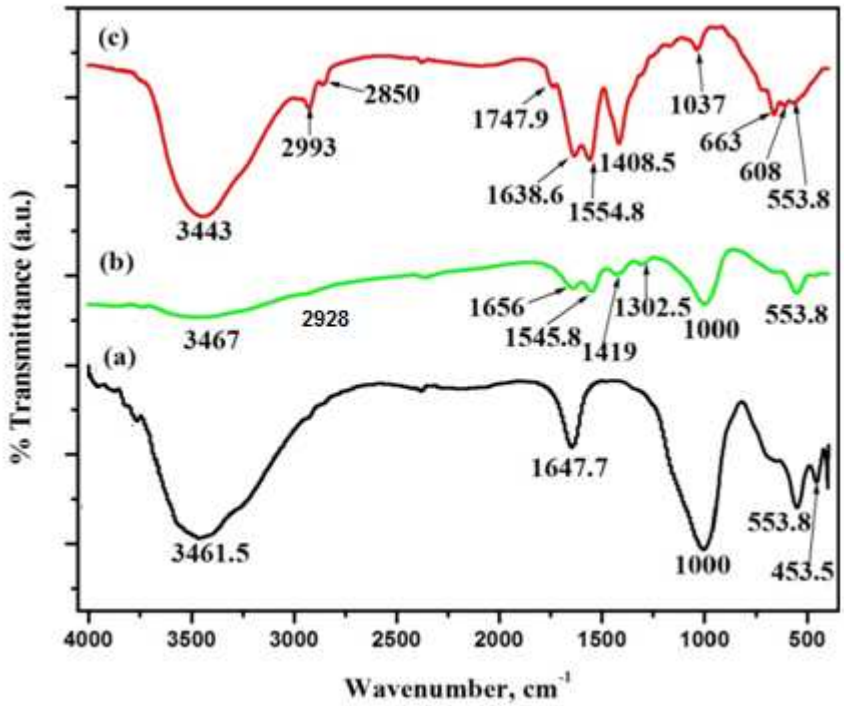

Figure 2. FTIR spectrum of a) Complex1 b) Complex 1-Y c) zeolite-Y.

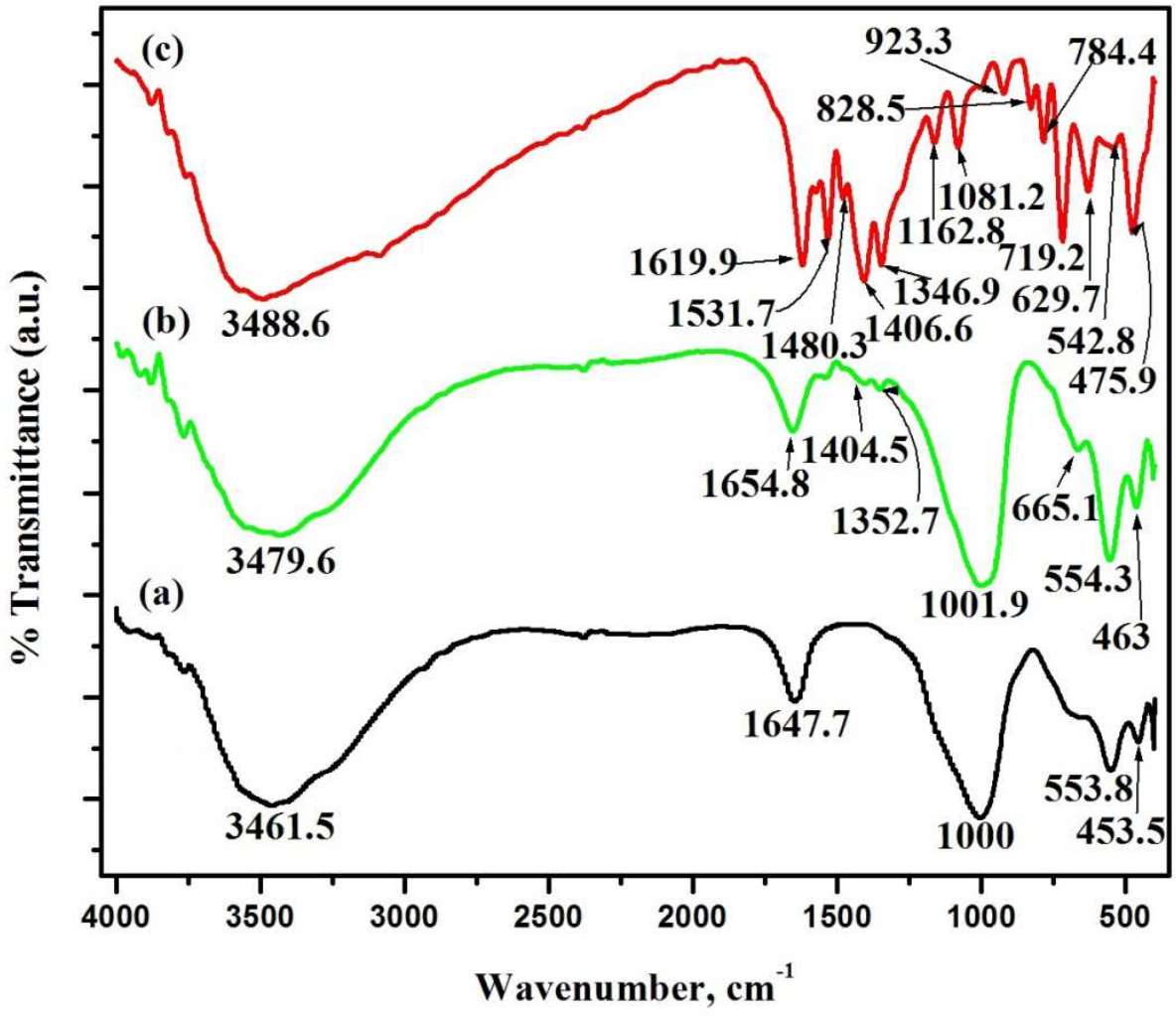

Figure 3. FTIR spectrum of a) Complex 2 b) Complex 2-Y c) zeolite-Y.

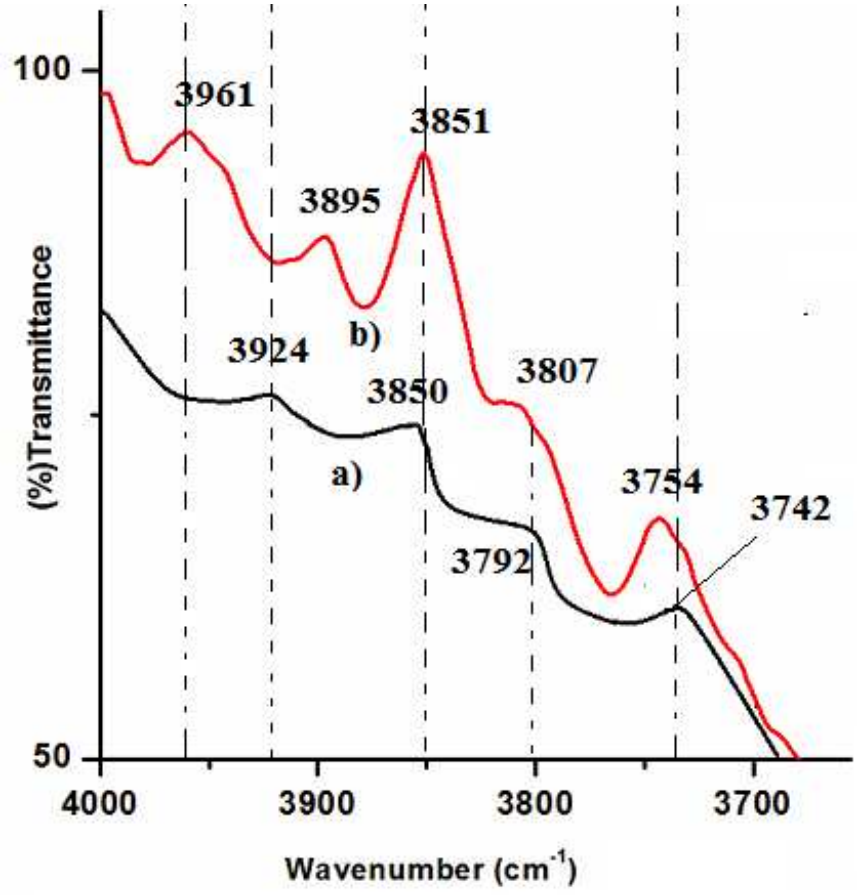

Figure 4. H-bonding region in zeolite supported a) Complex 1-Y and b) Complex 2-Y.

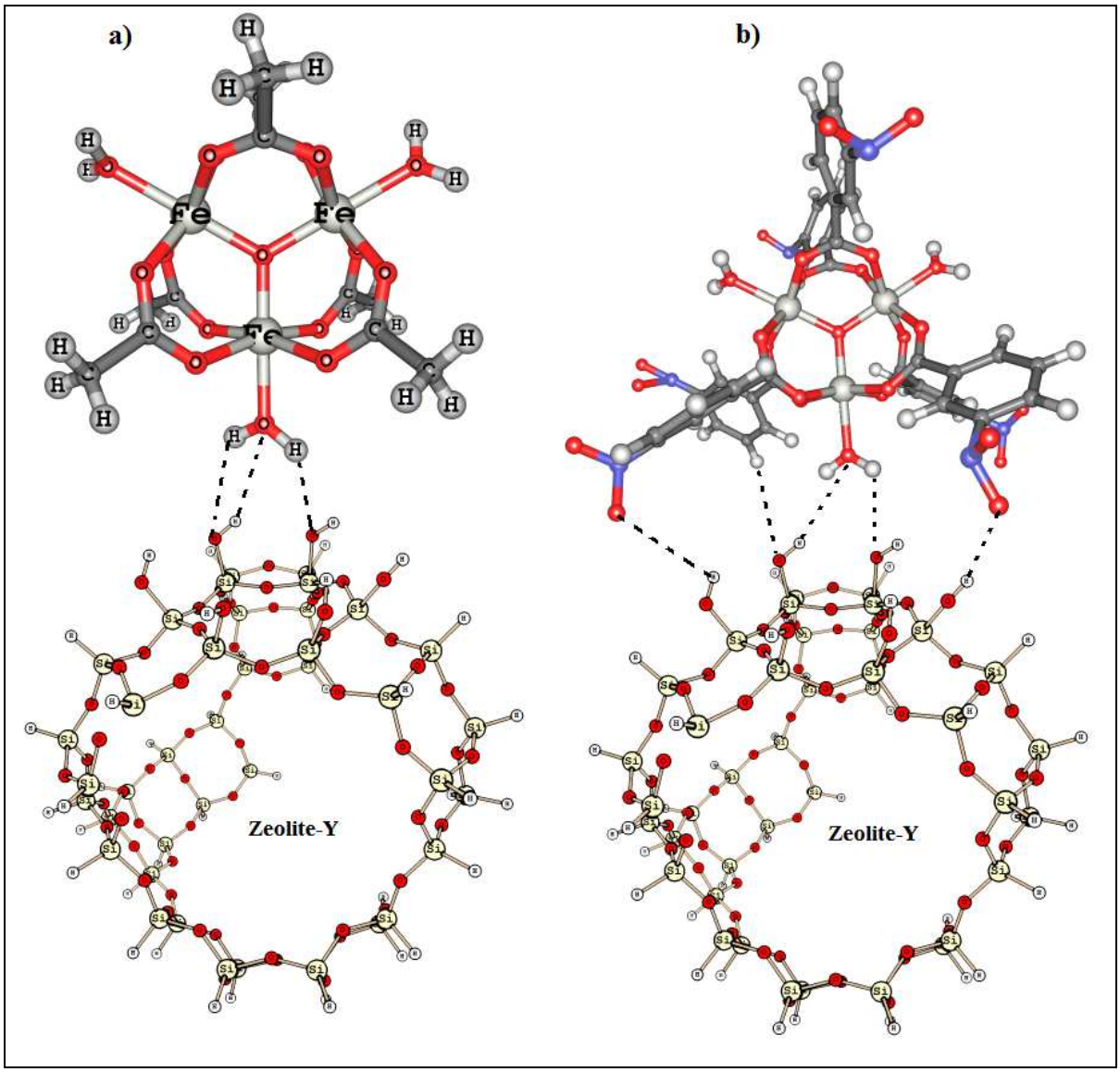

Figure 5. Probable H-bonding interaction between a) Complex 1, b) Complex 2 and zeolite-Y.

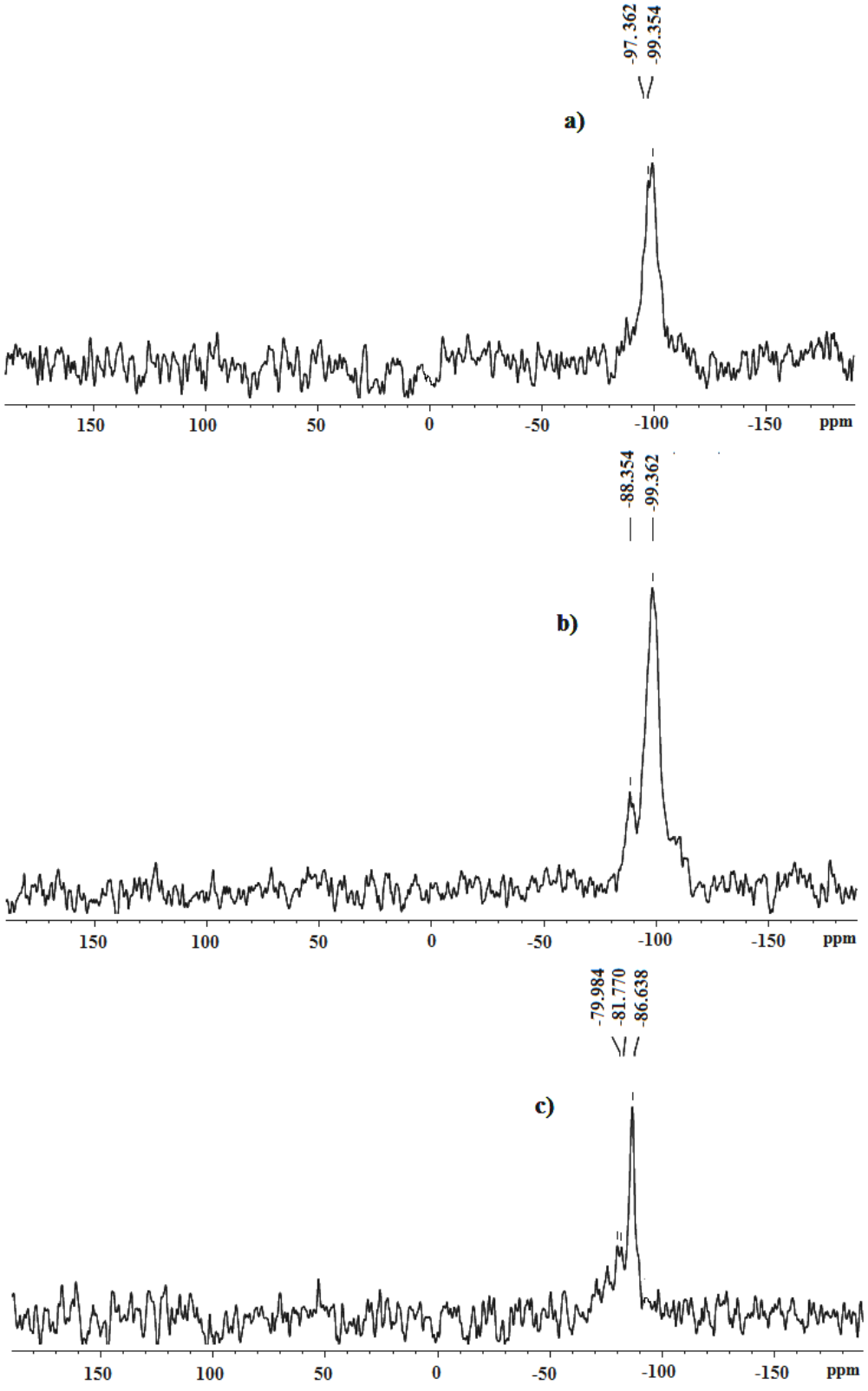

Figure 6. [29] Si NMR of a) Zeolite-Y b) Complex 1-Y and c) Complex 2-Y

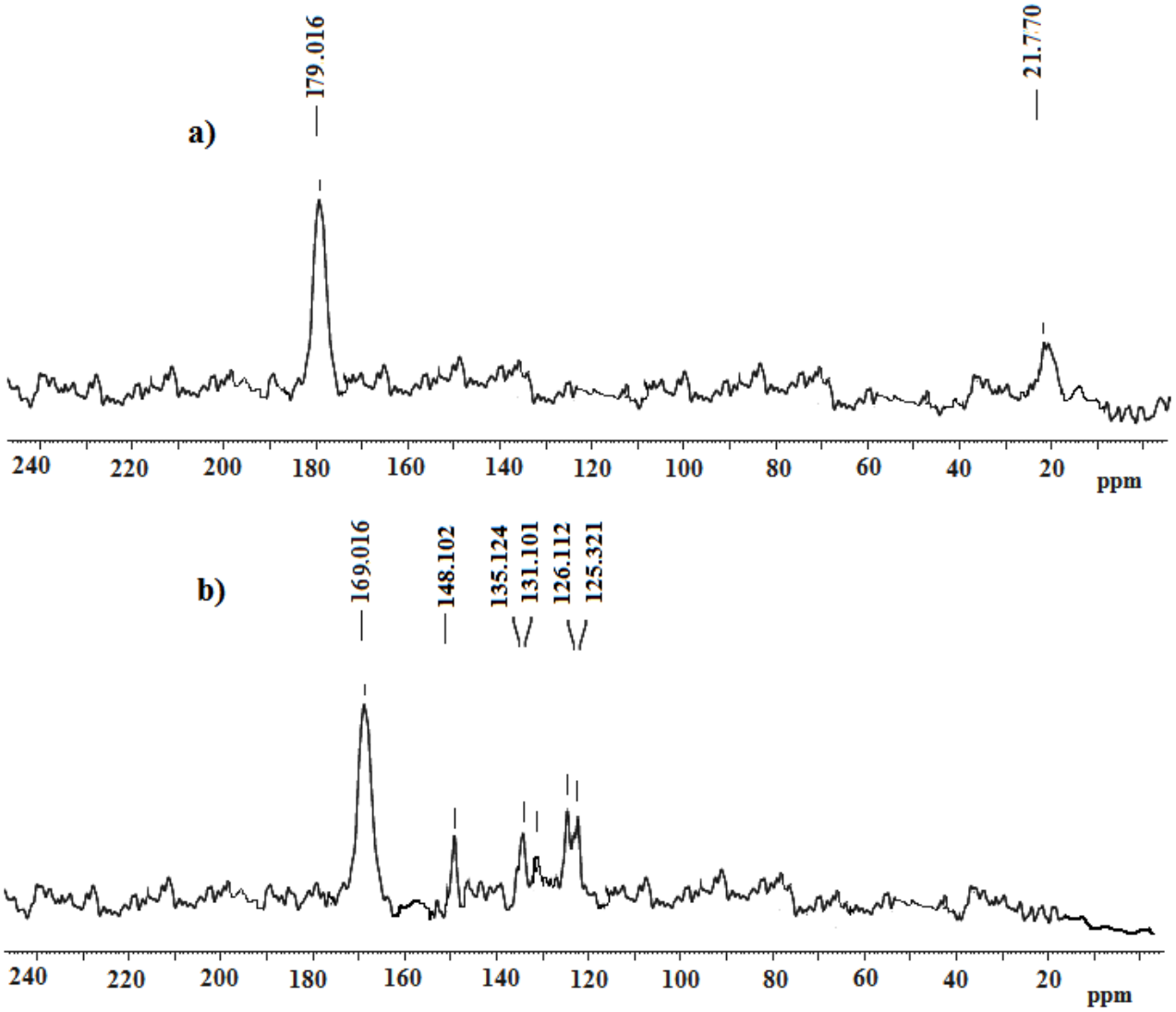

Figure 7. Solid state ^{13}C NMR of a) Complex 1-Y and b) Complex 2-Y

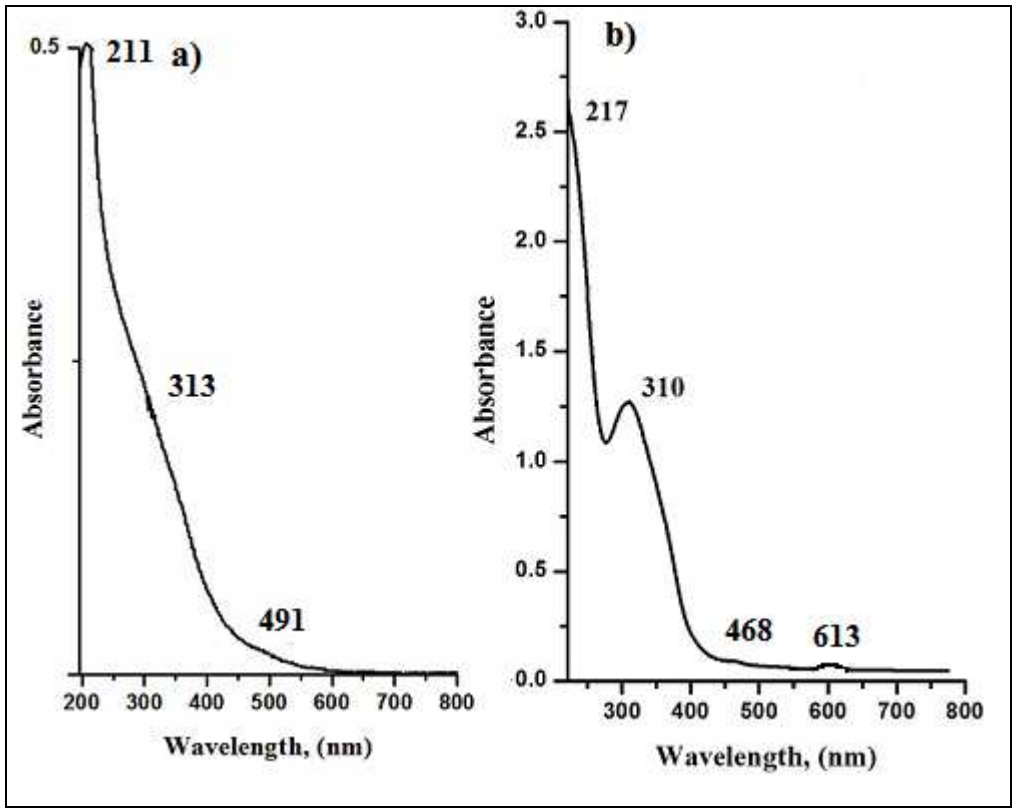

Figure 8. UV-vis spectrum of a) Complex 1 b) Complex 2 taken in solution phase.

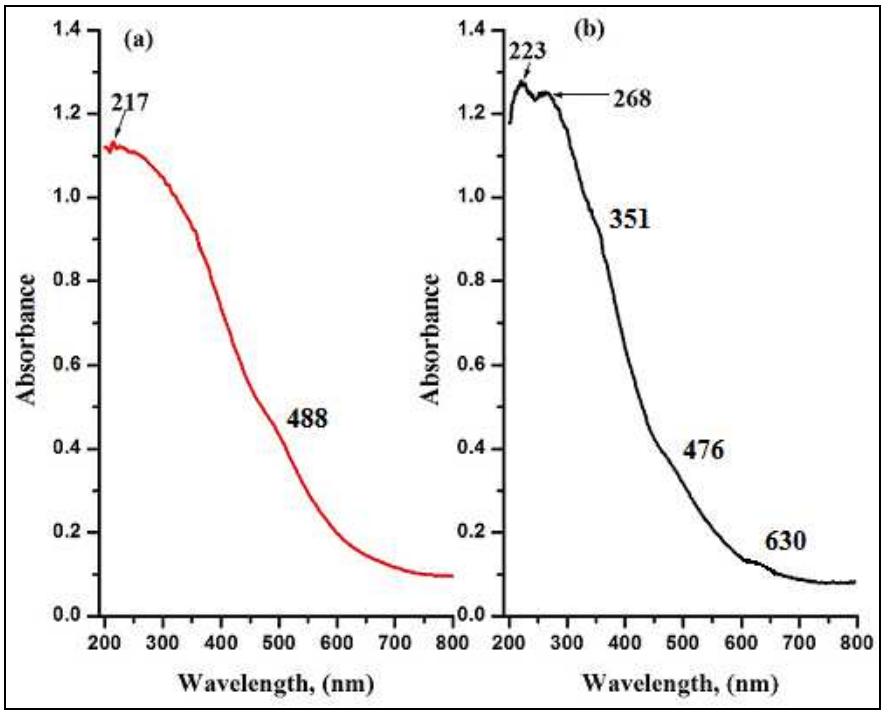

Figure 9. UV-vis/DRS of a) Complex 1-Y b) Complex 2-Y.

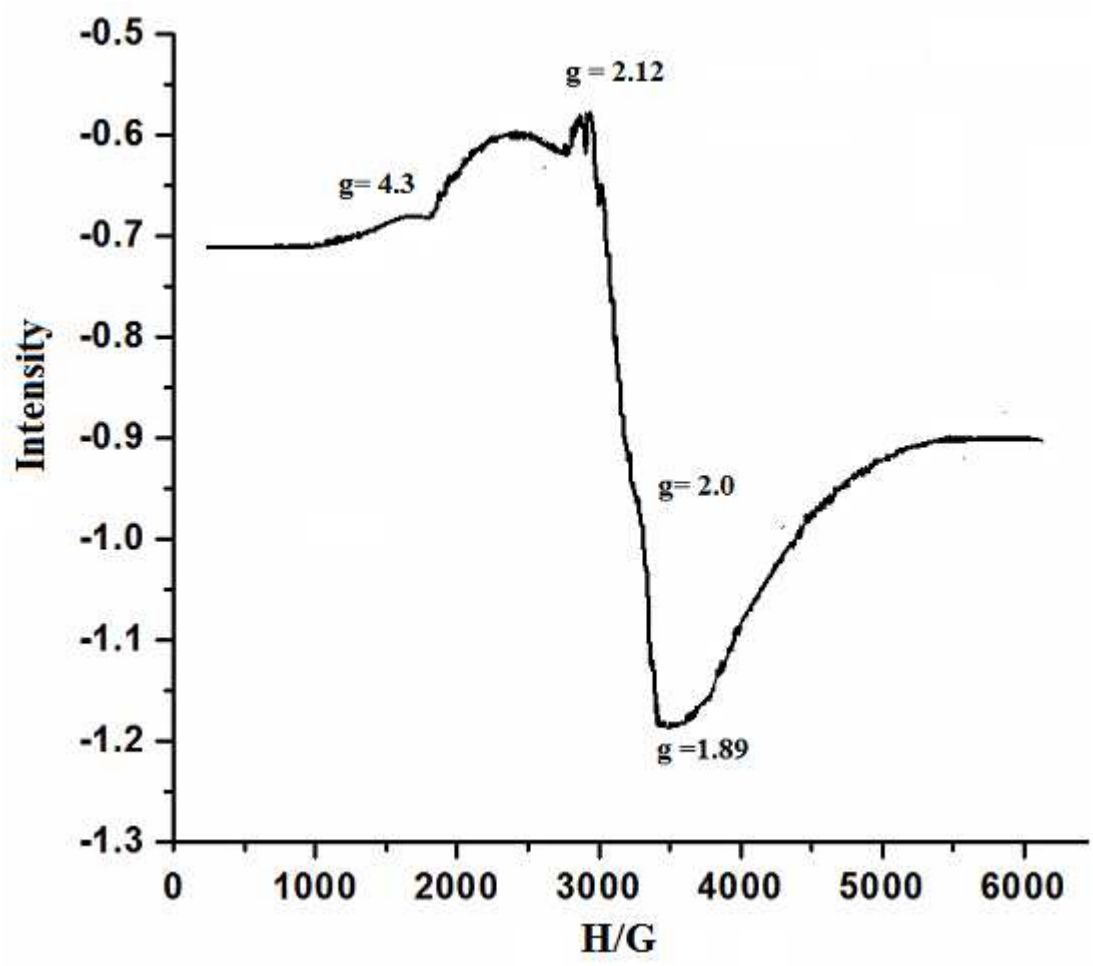

Figure 10. ESR spectrum of Complex 1-Y

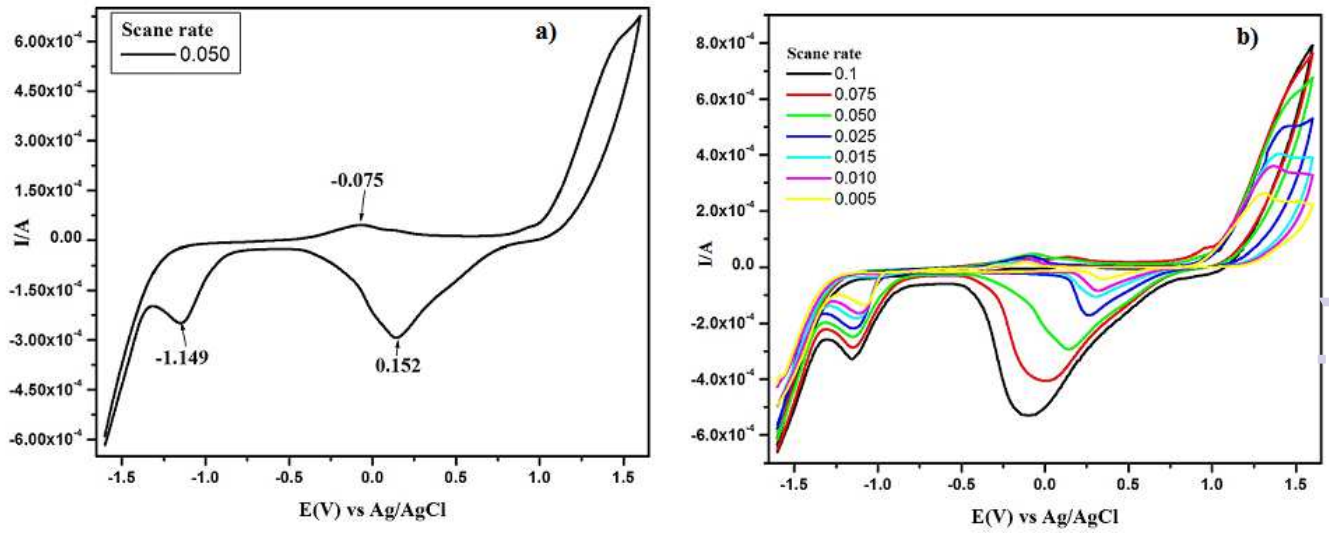

Figure 11. Cyclic voltammogram of a) Complex 1 and b) at different scan rate.

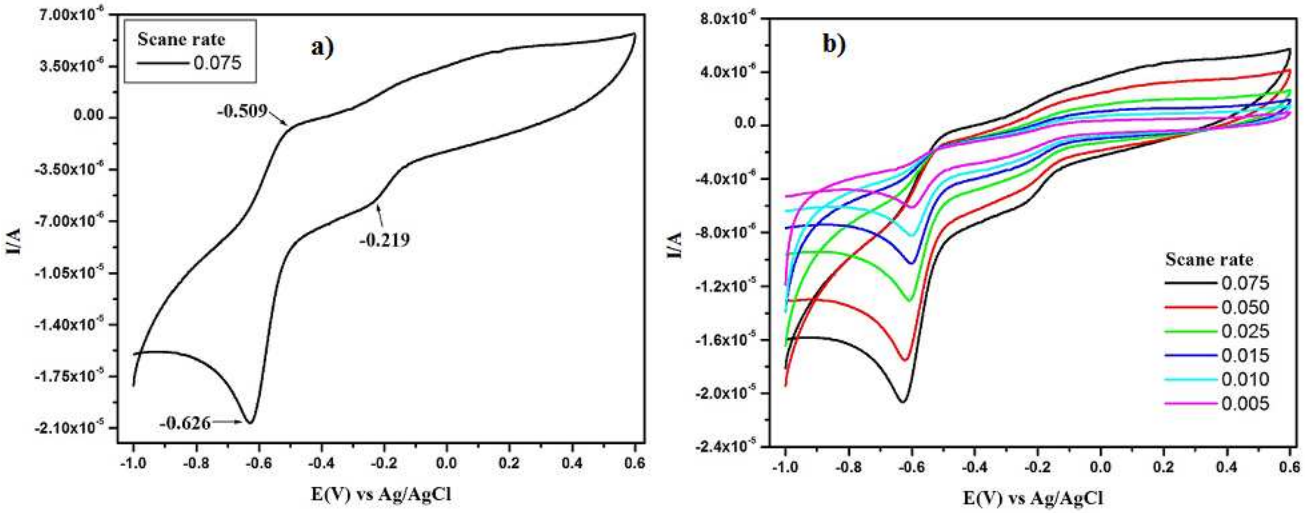

Figure 12. Cyclic voltammogram of a) Complex 1-Y b) at different scan rate.

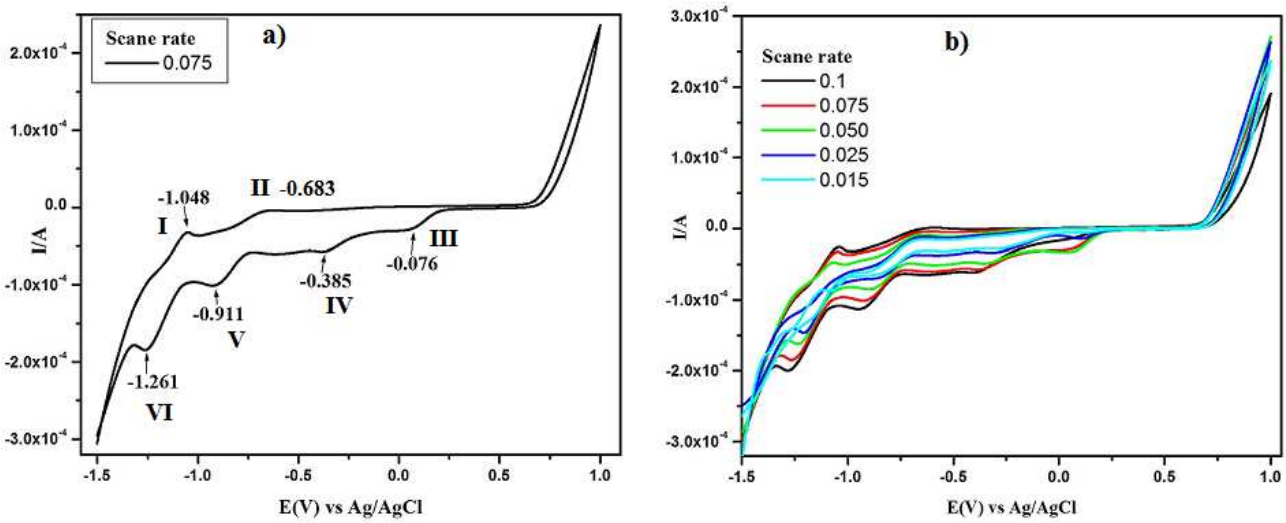

Figure 13. Cyclic voltammogram of a) Complex 2 b) at different scan rate.

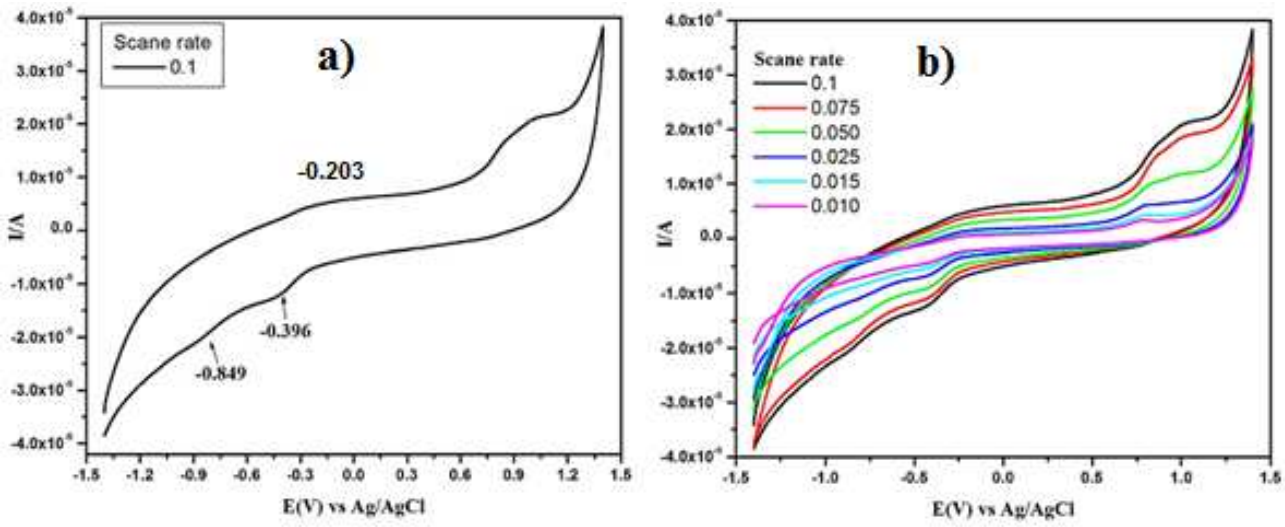

Figure 14. Cyclic voltammogram of a) Complex 2-Y b) at different scan rate.

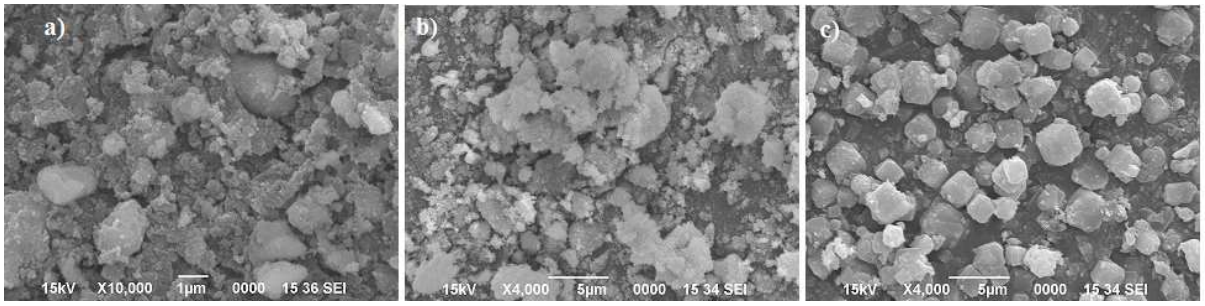

Figure 15. SEM image of a) Complex 1-Y b) Complex 2-Y c) Zeolite-Y.

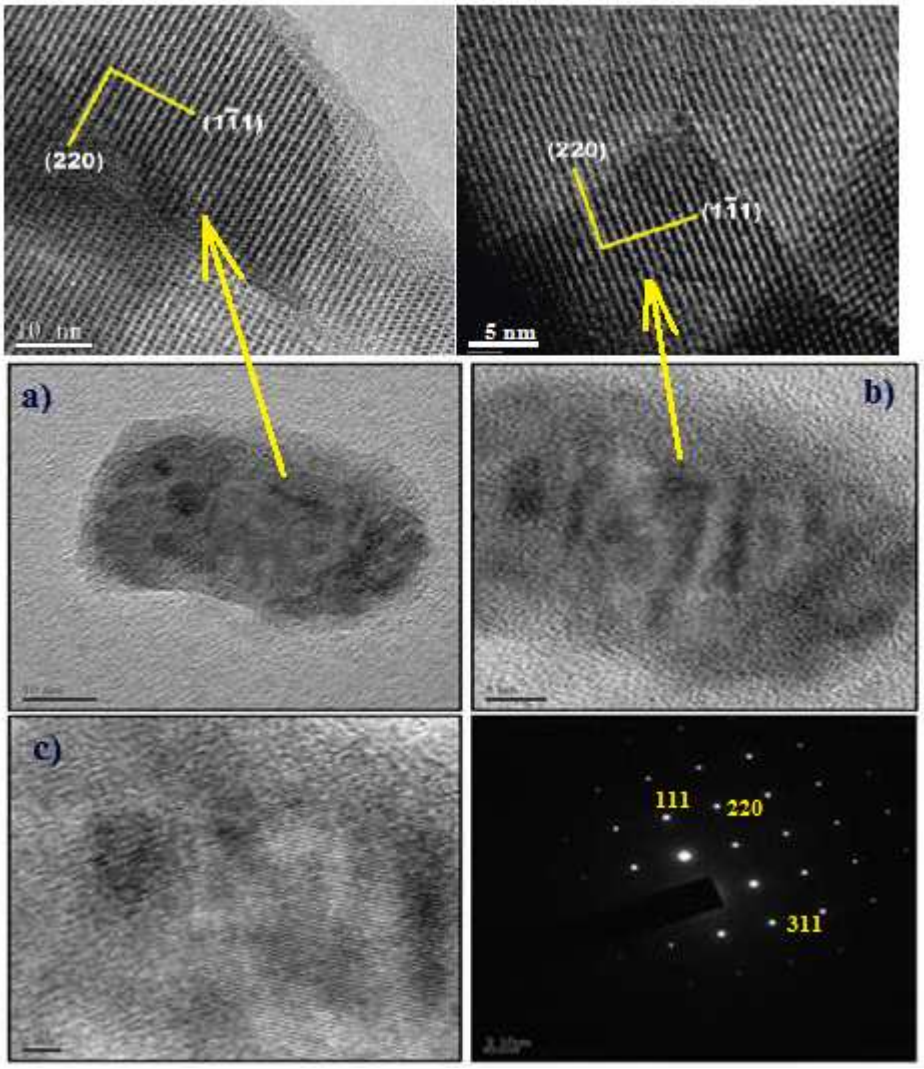

Figure 16. HRTEM of a) Complex 1-Y b) Complex 2-Y c) Zeolite-Y.

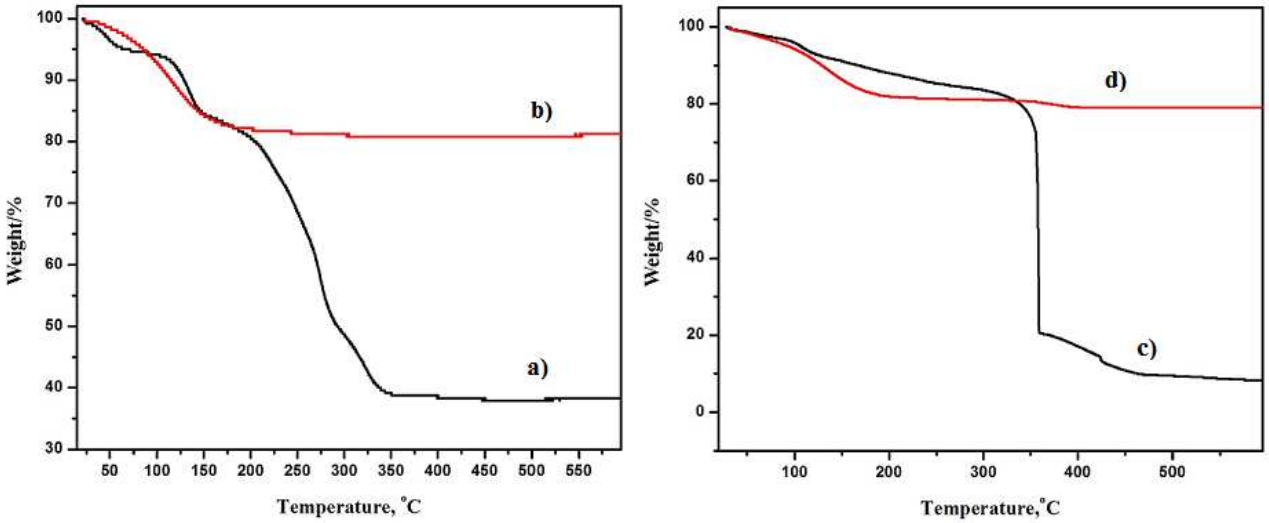

Figure 17. TGA analysis of a) Complex1 b) Complex1-Y c) Complex 2 d) Complex 2-Y.

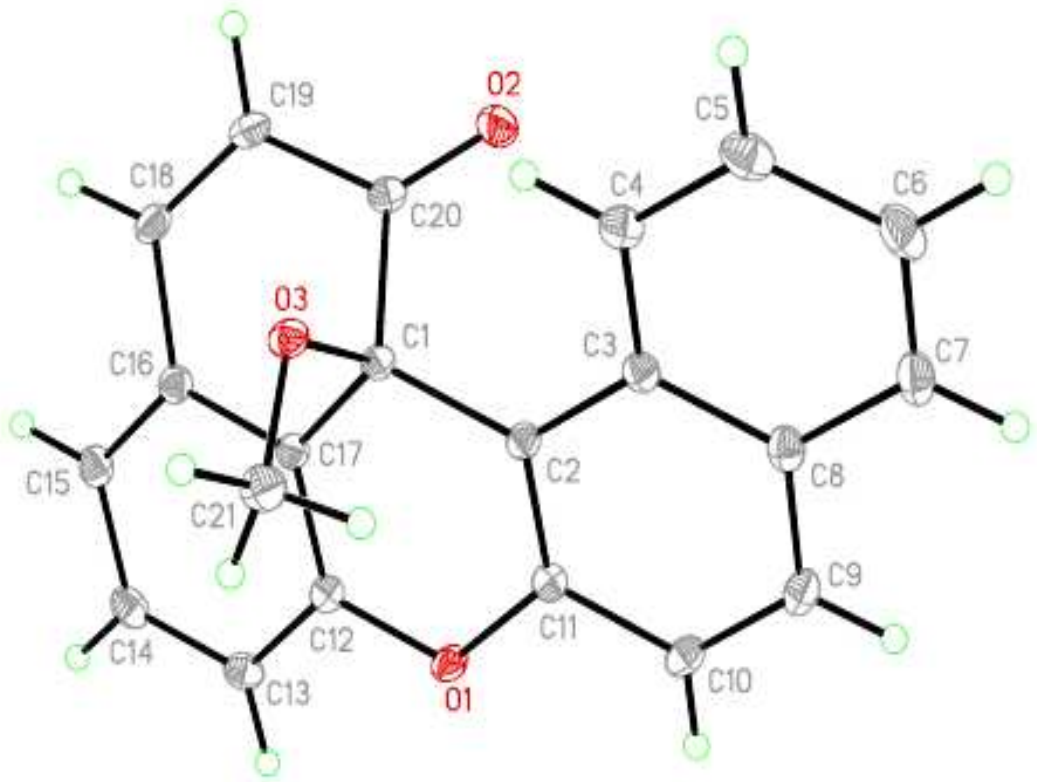

Figure 18. Crystal Structure of minor product.

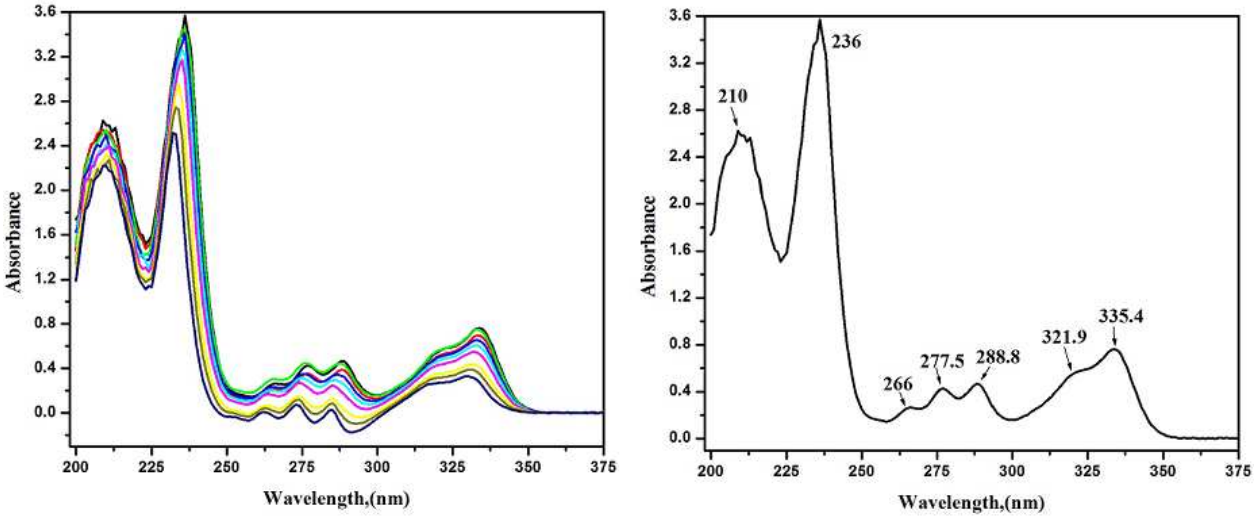

Figure 19. UV-vis study of catalytic conversion of 2 Naphthol to BINOL by Complex2-Y

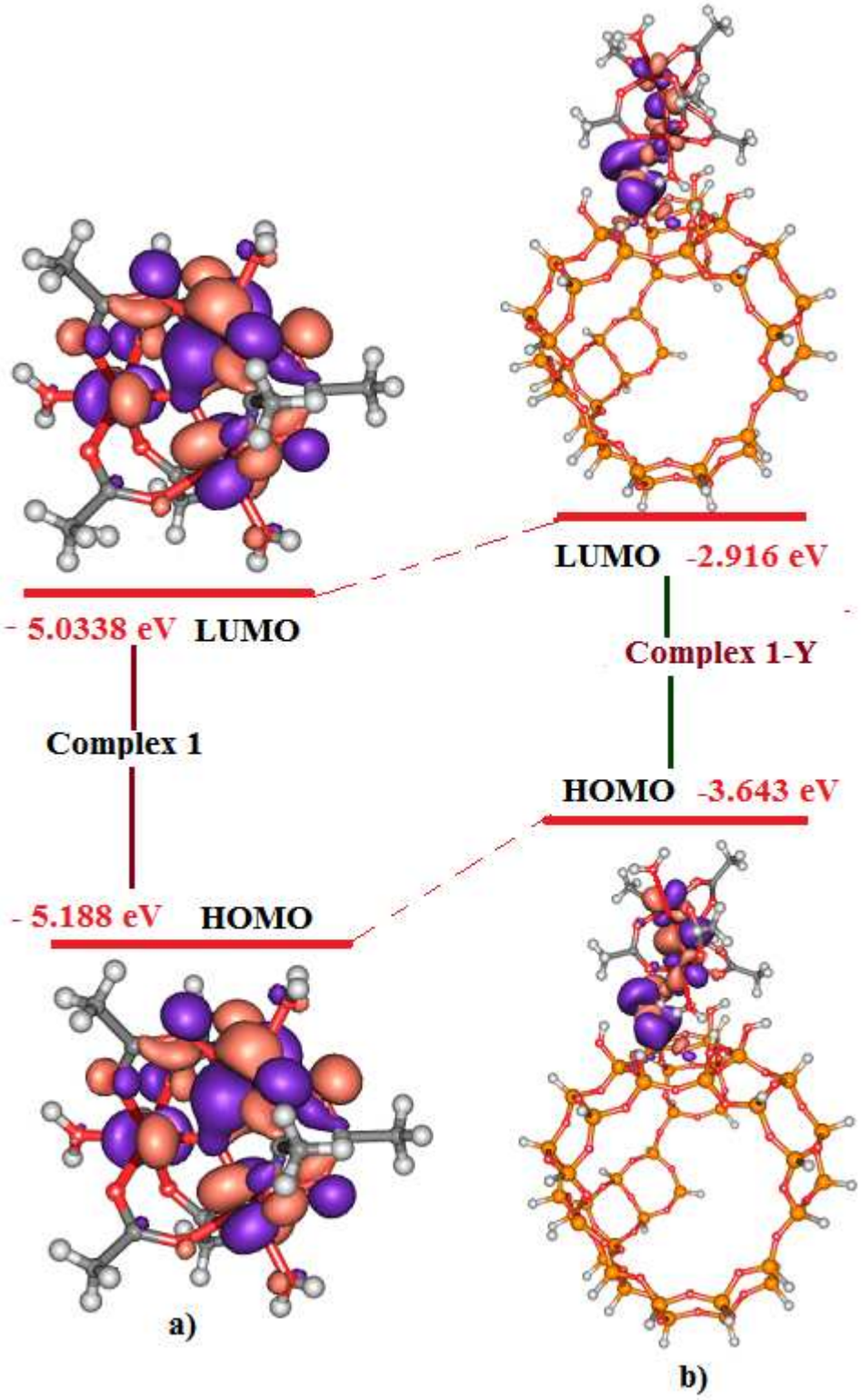

Figure 20. HOMO and LUMO orbitals in a) Complex 1 and b) Complex 1-Y.

TOC

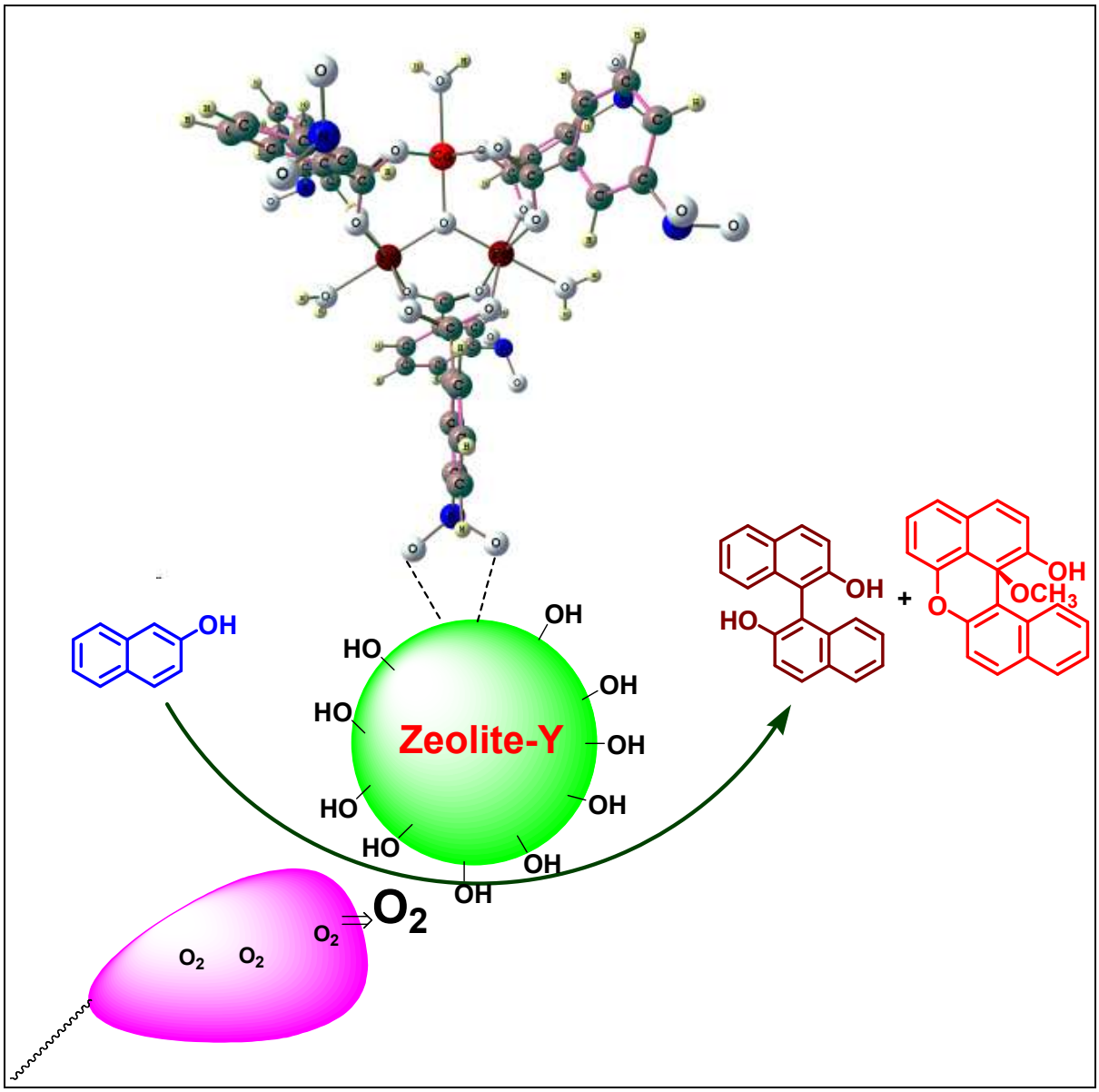

Trinuclear metal-oxo cluster supported on zeolite-Y is found to be effecient catalyst for oxidation of 2-naphthol to BINOL with high turn over frequency.